Brief Communications
Preprint
Academia Quantum

E_8 and H_4 in QM and QC

J Gregory Moxness

TheoryOfEverything.org
jgmoxness@TheoryOfEverything.org

Abstract

This paper 'with code' presents several notable properties of the matrix $\mathbb{U}$ shown to be related to the isomorphism between H_4 and E_8. The most significant of these properties is that $\mathbb{U}.\mathbb{U}$ is to rank 8 matrices what the golden ratio is to numbers. That is to say, the difference between it and its inverse is the identity element, albeit with a twist. Specifically, $\mathbb{U}.\mathbb{U}\text{-}(\mathbb{U}.\mathbb{U})^{-1}$ is the reverse identity matrix or standard involutory permutation matrix of rank 8. It has the same palindromic characteristic polynomial coefficients as the normalized 3-qubit Hadamard matrix with 8-bit binary basis states, which is known to be isomorphic to E_8 through its (8,4) Hamming code. This combined with finding the construction of $\mathbb{U}$ from the Pauli matrices' relationships to 2-qubit CNOT, SWAP and 3-qubit Toffoli CCNOT and Hadamard matrices will inform the understanding of group theoretic quantum mechanics (QM), quantum computing (QC), quantum chemistry, and particle physics.

Keywords Coxeter groups, root systems, E8

1 Introduction

Fig. 1 is the Petrie projection of the Gosset 4_{21} 8-polytope derived from the Split Real Even (SRE) form of the E_8 Lie group with unimodular lattice in $\mathbb{R}^8$. The reader may be familiar with some or all figures shown (e.g. in the corresponding Wikipedia articles on the topic). All were generated using author developed *Mathematica*™ (MTM) `VisibLie_E8` notebook source code and interactive user interface.

E_8 has 240 vertices and 6,720 edges of 8-dimensional (8D) length $\sqrt{2}$. E_8 is the largest of the exceptional simple Lie algebras, groups, lattices, and polytopes, and is related to octonions ($\mathbb{O}$), (8,4) Hamming codes, and 3-qubit (8 basis state) Hadamard matrix gates. An important and related higher dimensional structure is the $\mathbb{R}^{24}$ ($\mathbb{C}^{12}$) Leech lattice with its binary (ternary) Golay code construction ($\Lambda_{24} \supset E_8 \oplus E_8 \oplus E_8$ or $\mathbb{E}_8^3$ as the 23rd Niemeier lattice[1] in the Kneser neighborhood graph shown in Fig. 12).

The Leech lattice (Λ_{24}) is the largest of the Conway groups (Co_0) and is the group of automorphisms of three Leech lattice related sporadic groups $Aut(Co_1,Co_2,Co_3)$. As a lattice with no roots (i.e. with a Coxeter number of 0), it is at the top of the relationship map of the 24 Niemeier lattices as described in Table 2. The Y_{555} Coxeter-Dynkin diagram in Fig. 10 gives the quotient of the BiMonster group (BiM), which is the wreath product of the Monster group (M) with $\mathbb{Z}_2$ ($M \wr \mathbb{Z}_2$). With M as the largest member of the sporadic groups and E_8 as the largest member of the exceptional groups, each can be decomposed by showing sub-quotient relationships in a Hasse diagram, as shown Figs. 11 and 13

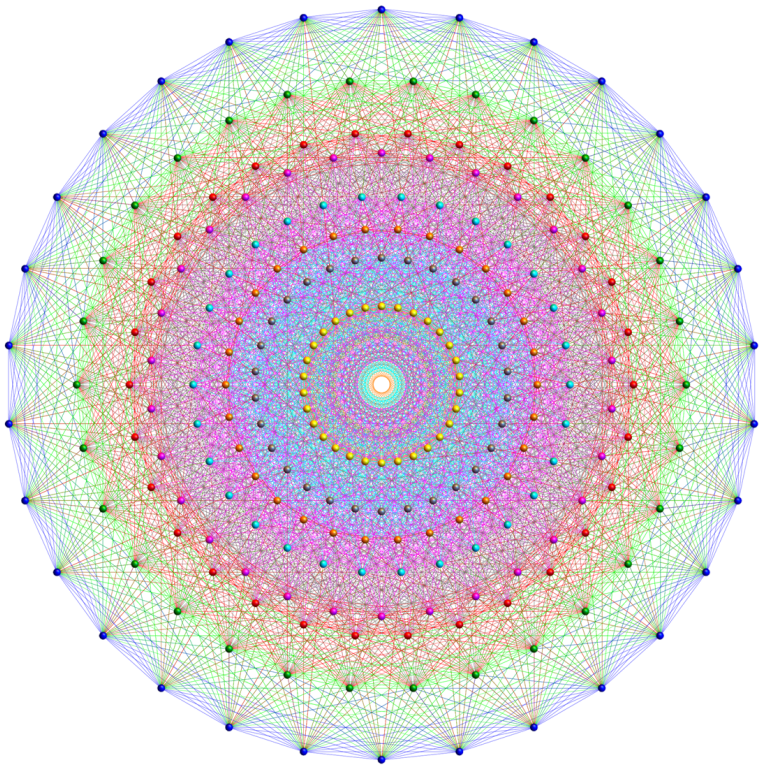

Figure 1: E_8 4_{21} Petrie projection with 8 concentric rings of 30 vertices which are in the same color palette used to color the edges, which uses an algorithm that assigns colors based on the norm of the projected edge. The vertex ring colors from smallest to largest are: 1=Yellow,2=Gray,3=Orange,4=Cyan,5=Magenta,6=Red,7=Green,8=Blue.
The pattern is based on 2 golden ratio (φ) scaled sets of 4 rings of 30 600-cell vertices in Van Oss projection (i.e. H4 rings 1,3,4,5 and H4φ rings 2,6,7,8). Each ring of 30 contains 1 on-XY-axis vertex with its reflection vertices as a 16-cell and 2 off-XY-axis vertices with their reflections as an 8-cell in 4 rings making up the 24-cell. This is combined with 4 24-cell rotations of $\pi/5$ making up the snub 24-cell of 96 vertices. See Fig. 7 a) and b) for a more detailed visualization of the 4-polytope sub-structure represented in this E_8 diagram. Each ring forms a 4D Boerdijk-Coxeter that tessellates the 3-sphere surface of the 600-cell as shown in Fig. 1c and d.

respectively. In terms of the triality of the Y_{abc} Coxeter-Dynkin diagram, of interest here for example are the self-dual D_4 24-cell as Y_{111} and E_8 as Y_{421}.

The Coxeter-Dynkin diagram for E_8 is shown in Fig. 2 along with its Cartan matrix (`cmE8`) and simple roots matrix (`srE8`). It is easy to show that `cmE8`=`srE8.srE8`^{T}, such that we can think of the simple roots as $\sqrt{\texttt{cmE8}}$. It was also shown that the SRE E_8 vertex coordinates can be derived from the dot product of $\pm$`E8roots.srE8`. Applying these relationships to $\mathbb{U}$ gives interesting results as described in Section 3.

The quaternion ($\mathbb{H}$) Weyl group orbit O(Λ)=W(H_4)=I of order 120 is constructed from the parent orbit (1000) of the Coxeter-Dynkin diagram for H_4 shown in Fig. 3b. This results in the 600-cell 4-polytope of order 120 labeled here and in [2] as I. In Section 2, it will be shown that $\mathbb{U}$ provides for a direct mapping from E_8 to four copies $(1 \oplus \varphi)(H4_L \oplus H4_R)$ of both the 600-cell and the tri-rectified parent of H_4 (i.e. the filled node 1 is shifted right 3 times giving 0001), which is the 120-cell of order 600 labeled here and in [2] as J. Both of these 4-polytopes are shown in Figs. 8-9 as concentric 3D hulls.

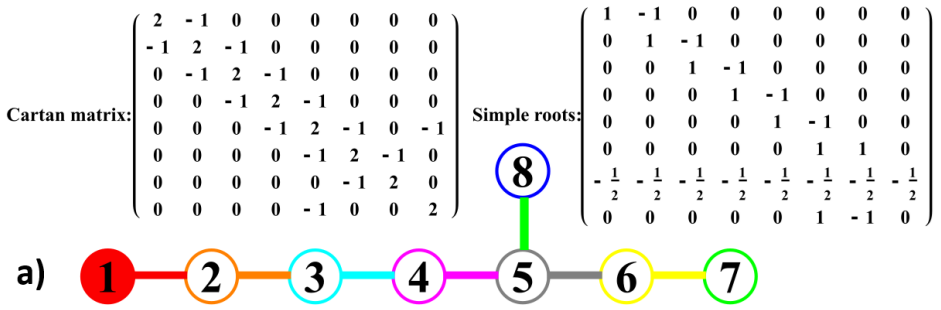

Figure 2: a) E_8 Coxeter-Dynkin diagram with it Cartan matrix and simple roots matrix

It has been shown[3] that the matrix $\mathbb{U}$ in (1) along with its inverse (2) is related to the isomorphism between H_4 and E_8.

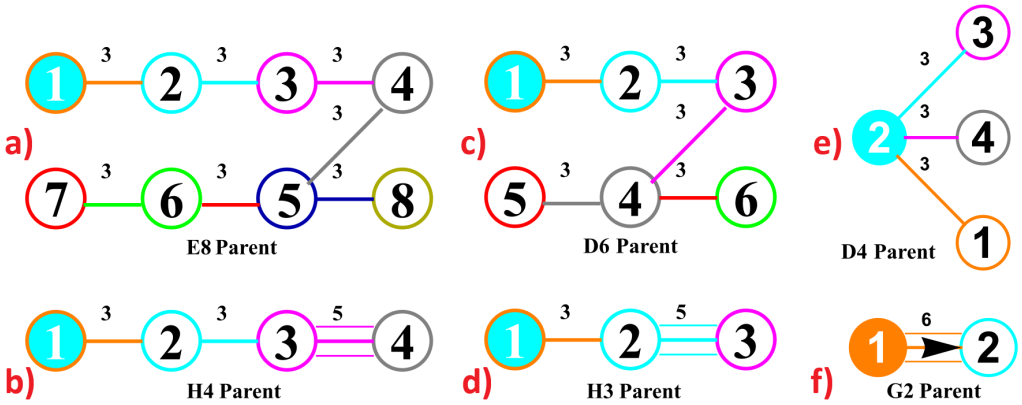

Figure 3: Coxeter-Dynkin diagram folding patterns
a) E_8 in folding orientation
b) The associated folded H_4 ≅600-cell
c) D_6 in folding orientation
d) The associated folded H_3
e) D_4 ≅24-cell in folding orientation
f) The associated folded $G_2 \cong Aut(\mathbb{O})$

It is known[4] that the E_8 can be projected, mapped, or "folded" (as shown in Fig. 3a and b) to two golden ratio $\varphi = \frac{1}{2}\left(1+\sqrt{5}\right) \approx 1.618$ scaled copies of the 4 dimensional 120 vertex 720 edge H_4 600-cell. Folding an 8D object into a 4D one can be done by projecting each vertex using its dot product with a 4×8 matrix (e.g. using the first or last 4 rows or columns of $\mathbb{U}$). This produces $H_4 \oplus \varphi H_4$, where H_4 is the binary icosahedral group $2I$ of order 120, a subgroup of Spin(3). It covers H_3 as the full icosahedral group I_h of order 120, a subgroup of SO(3). The binary icosahedral group is the double cover of the alternating group A_5.

2 Constructing the palindromic unitary matrix $\mathbb{U}$

Despite others'[5][6] recent attempts, the inverse morphism or "unfolding" from H_4 to E_8 is less trivial given that the matrix is not square and lacks an inverse. Yet, a real ($\mathbb{R}$) symmetric volume preserving Det($\mathbb{U}$)=1 rotation matrix(1) was derived in 2012 and documented[3]. The quadrant structure of $\mathbb{U}$ rotates E_8 into four 4D copies of H_4 600-cells, with the original two (L)eft and (R)ight side unit scaled 4D copies related to the two L/R

φ scaled copies. This traceless form of $\mathbb{U}$ has palindromic characteristic coefficients and provides for an explicit isomorphic mapping of $E_8 \leftrightarrow (1 \oplus \varphi)(H4_L \oplus H4_R)$ which involves using a bidirectional L↔R mapping function (`mapLR`) and $\mathbb{U}^{-1}(2)$.

It is interesting to note the exchange of $1 \leftrightarrow \varphi$ in $\mathbb{U} \leftrightarrow \mathbb{U}^{-1}$, excluding $-\varphi^2$. The properties of $\mathbb{U}$ are described in more detail in Section 3.

$$\mathbb{U} = \begin{pmatrix} 1-\varphi & 0 & 0 & 0 & 0 & 0 & 0 & -\varphi^2 \\ 0 & -1 & \varphi & 0 & 0 & \varphi & 1 & 0 \\ 0 & \varphi & 0 & 1 & -1 & 0 & \varphi & 0 \\ 0 & 0 & -1 & \varphi & \varphi & 1 & 0 & 0 \\ 0 & 0 & 1 & \varphi & \varphi & -1 & 0 & 0 \\ 0 & \varphi & 0 & 1 & -1 & 0 & \varphi & 0 \\ 0 & 1 & \varphi & 0 & 0 & \varphi & -1 & 0 \\ -\varphi^2 & 0 & 0 & 0 & 0 & 0 & 0 & 1-\varphi \end{pmatrix} /(2\sqrt{\varphi}) \tag{1}$$

$$\mathbb{U}^{-1} = \begin{pmatrix} \varphi-1 & 0 & 0 & 0 & 0 & 0 & 0 & -\varphi^2 \\ 0 & -\varphi & 1 & 0 & 0 & 1 & \varphi & 0 \\ 0 & 1 & 0 & \varphi & -\varphi & 0 & 1 & 0 \\ 0 & 0 & -\varphi & 1 & 1 & \varphi & 0 & 0 \\ 0 & 0 & \varphi & 1 & 1 & -\varphi & 0 & 0 \\ 0 & 1 & 0 & \varphi & -\varphi & 0 & 1 & 0 \\ 0 & \varphi & 1 & 0 & 0 & 1 & -\varphi & 0 \\ -\varphi^2 & 0 & 0 & 0 & 0 & 0 & 0 & \varphi-1 \end{pmatrix} /(2\sqrt{\varphi}) \tag{2}$$

$\mathbb{U}$ can be generated using a combination of the unimodular matrices commonly used for QC logic, namely those of the 2-qubit CNOT (3) and SWAP (4) gates. Taking these patterns, combined with the recursive functions that build φ from the Fibonacci sequence, it is straightforward to derive $\mathbb{U}$ from scaled QC logic gates[3].

$$\text{CNOT} = \begin{pmatrix} 1 & 0 & 0 & 0 \\ 0 & 1 & 0 & 0 \\ 0 & 0 & 0 & 1 \\ 0 & 0 & 1 & 0 \end{pmatrix} \tag{3}$$

$$\text{SWAP} = \begin{pmatrix} 1 & 0 & 0 & 0 \\ 0 & 0 & 1 & 0 \\ 0 & 1 & 0 & 0 \\ 0 & 0 & 0 & 1 \end{pmatrix} \tag{4}$$

The particular maximal embedding of E_8 at height 248 that we are interested in for this work is shown in Fig. 14 as the special orthogonal group of SO(16)≅D_8 at height (120=112+4+4)+128‘, where 112 is interpreted as the subgroup embeddings of SO(8)⊗SO(8)≅$D_4 \otimes D_4$ and 128‘ is interpreted as symplectic subgroup embeddings of C_8 where Sp(8)⊗Sp(8)≅$C_4 \otimes C_4$ at height 136=128+4+4. These selected embeddings correspond to the 112 integer D_8 vertices and the 128 half-integer BC_8 (the 8-demicube) vertices given by SRE E_8, in addition to the $8 \oplus \overline{8}$ generator roots for a total of 2^8. This is in 1::1 correspondence with the canonical root vertex ordering from the 9th row of the palindromic Pascal triangle $\{1, 8, 28, 56, 35\overline{35}, \overline{56}, \overline{28}, \overline{8}, \overline{1}\}$, where each entry in the list gives the number of vertices that alternate between half-integer BC_8 and integer D_8 vertex sets, with the right 5 overbar sets of 128 vertices being the negated vertices of the left 5 sets of 128 in reverse order.

At this point it is interesting to note the connection between $E_8 \cong BC_8 \oplus D_8$ and H_4 quasicrystals. If we project E_8 into the Petrie projection of the D_6 Coxeter plane, which has the same 10 dihedral symmetry basis as the BC_6 6-demicube and 5-cube, and overlay that with the electron diffraction pattern of an icosahedral Zn-Mg-Ho QuasiCrystal, the resonances in the diffractogram are striking in the pattern matching to the E_8 vertex overlap counts and the edges that meet between the vertex rings. This makes sense due to the fact that D_6 folds to H_3 as shown in shown in Fig. 3c and d. So even quantum chemistry is informed by the symmetry of E_8 and its subgroups.

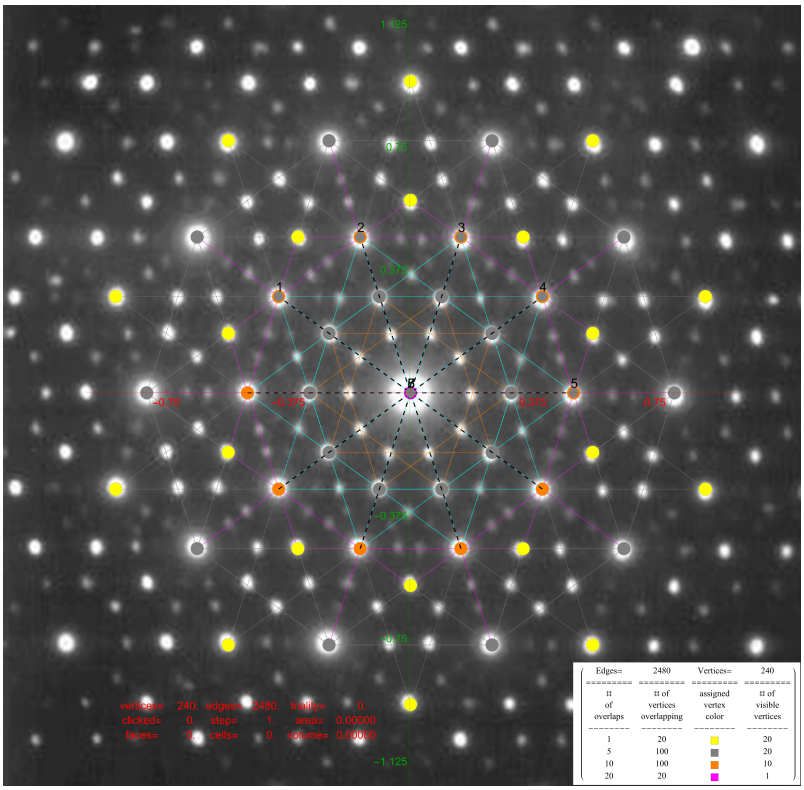

Figure 4: Icosahedral Zn-Mg-Ho QuasiCrystal
There are 2480 overlapping edge lines from the 240 E_8 vertices. They have unit norm lengths calculated from the 5D non-zero projected dimensions of E_8. Of these, 32 inner vertices and 80 edges belong to the 5D 5-Cube (Penteract) proper. Edges are shown with colors assigned based on origin vertex distance from the outer perimeter. The vertex colors of the 5-Cube projection represent E8 vertex overlaps.

These embeddings have an isomorphic connection to $\mathbb{U}$ and provide the $E_8 \leftrightarrow (1 \oplus \varphi)(H4_L \oplus H4_R)$ mapping via `mapLR`. It demonstrates that E_8 rotates into four 4D copies of H_4 600-cells, with the original two (L)eft side φ scaled 4D copies related to the two (R)ight side unscaled 4D copies.

Due to the palindromic structure of $\mathbb{U}$, the H_{4L} and H_{4R} are also palindromic with each R vertex being the reverse order of the L vertex, along with `mapLR` exchanges in the (S)nub 24-cell vertices. For each L vertex that is not a member of the (T)etrahedral group's self-dual D_4 24-cell (or φT), the R vertex will be a member of the scaled φS (or S) respectively. This is due to the exchange of $\varphi^{3/2} \leftrightarrow \varphi^{-3/2}$ in `mapLR` which changes the norm (i.e. to/from a small norm$=1/\sqrt{\varphi}$ or a large norm$=\sqrt{\varphi}$). The 24-cell T vertices are unaffected by `mapLR` exchange and have L and R vertex values of the same norm and palindromic opposite entries, with the larger φH_4 having the same signs and the smaller unit scaled H_4 having opposite signs.

3 Properties of $\mathbb{U}$

Similar to the relationships between the Cartan matrix, ±roots, weights, heights of E_8, we can construct a Cartan matrix $\mathtt{cm}\mathbb{U}$=$\mathbb{U}.\mathbb{U}$ shown in (5), with $\mathbb{U}$ playing the role of the simple roots matrix. Just as the integer identity φ-$1/\varphi$=1, we now have $\mathtt{cm}\mathbb{U}$-$\mathtt{cm}\mathbb{U}^{-1}$ generating the exchange matrix or standard involutory permutation matrix of rank 8 shown in (6). This has the same palindromic characteristic polynomial coefficients (10) as the normalized 3-qubit Hadamard matrix with 8-bit binary basis states shown in (7), which has been shown by Elkies[7] to be isomorphic to E_8 through its (8,4) Hamming code.

$$\mathtt{cm}\mathbb{U}=\begin{pmatrix} \frac{\sqrt{5}}{2} & 0 & 0 & 0 & 0 & 0 & 0 & \frac{1}{2} \\ 0 & \frac{\sqrt{5}}{2} & 0 & 0 & 0 & 0 & \frac{1}{2} & 0 \\ 0 & 0 & \frac{\sqrt{5}}{2} & 0 & 0 & \frac{1}{2} & 0 & 0 \\ 0 & 0 & 0 & \frac{\sqrt{5}}{2} & \frac{1}{2} & 0 & 0 & 0 \\ 0 & 0 & 0 & \frac{1}{2} & \frac{\sqrt{5}}{2} & 0 & 0 & 0 \\ 0 & 0 & \frac{1}{2} & 0 & 0 & \frac{\sqrt{5}}{2} & 0 & 0 \\ 0 & \frac{1}{2} & 0 & 0 & 0 & 0 & \frac{\sqrt{5}}{2} & 0 \\ \frac{1}{2} & 0 & 0 & 0 & 0 & 0 & 0 & \frac{\sqrt{5}}{2} \end{pmatrix} \tag{5}$$

$$\mathtt{cm}\mathbb{U}-\mathtt{cm}\mathbb{U}^{-1}=\begin{pmatrix} 0 & 0 & 0 & 0 & 0 & 0 & 0 & 1 \\ 0 & 0 & 0 & 0 & 0 & 0 & 1 & 0 \\ 0 & 0 & 0 & 0 & 0 & 1 & 0 & 0 \\ 0 & 0 & 0 & 0 & 1 & 0 & 0 & 0 \\ 0 & 0 & 0 & 1 & 0 & 0 & 0 & 0 \\ 0 & 0 & 1 & 0 & 0 & 0 & 0 & 0 \\ 0 & 1 & 0 & 0 & 0 & 0 & 0 & 0 \\ 1 & 0 & 0 & 0 & 0 & 0 & 0 & 0 \end{pmatrix} \tag{6}$$

$$H=\begin{pmatrix} 1 & 1 & 1 & 1 & 1 & 1 & 1 & 1 \\ 1 & -1 & 1 & -1 & 1 & -1 & 1 & -1 \\ 1 & 1 & -1 & -1 & 1 & 1 & -1 & -1 \\ 1 & -1 & -1 & 1 & 1 & -1 & -1 & 1 \\ 1 & 1 & 1 & 1 & -1 & -1 & -1 & -1 \\ 1 & -1 & 1 & -1 & -1 & 1 & -1 & 1 \\ 1 & 1 & -1 & -1 & -1 & -1 & 1 & 1 \\ 1 & -1 & -1 & 1 & -1 & 1 & 1 & -1 \end{pmatrix} /\sqrt{8} \tag{7}$$

Just as $\frac{\varphi+1/\varphi}{2\varphi-1}$=1, $\frac{\mathtt{cm}\mathbb{U}+\mathtt{cm}\mathbb{U}^{-1}}{2\varphi-1}$=8x8 Identity Matrix. Of course, we can reverse the rows in $\mathtt{cm}\mathbb{U}$, which then swaps the sum and difference operation results of Identity vs. Involutory permutation matrices (respectively). Also as the exponentiation of sum (difference) $\varphi^n \pm 1/\varphi^n$ results in integer factors on even (odd) n and integer radicand factors on odd (even) n as shown in Table 1, by using matrix power operations on $\mathtt{cm}\mathbb{U}^{\mathtt{n}} \pm \mathtt{cm}\mathbb{U}^{-n}$ produces the Identity (Involutory) matrices with those same scaling factors. This application of matrix powers to $\mathbb{U}$ instead of $\mathtt{cm}\mathbb{U}$ puts all even n as the alternating integer (integer radicand) matrices, with odd n shown in (8) and (9). Please note that like the 3-qubit Hadamard matrix, inside the square brackets these matrices are traceless and unitary with the characteristic polynomial of (10) and can be constructed from sums of Pauli matrices.

Table 1: Sum and difference in powers of φ

n	φ^n	φ^{-n}	$\varphi^n+\varphi^{-n}$	$\varphi^n-\varphi^{-n}$
1	φ	$\frac{1}{\varphi}$	$\sqrt{5}$	1
2	φ^2	$\frac{1}{\varphi^2}$	3	$\sqrt{5}$
3	φ^3	$\frac{1}{\varphi^3}$	$2\sqrt{5}$	4
4	φ^4	$\frac{1}{\varphi^4}$	7	$3\sqrt{5}$
5	φ^5	$\frac{1}{\varphi^5}$	$5\sqrt{5}$	11

$$\mathbb{U}^{odd(n)}+\mathbb{U}^{-odd(n)}=\left[\mathtt{u}\mathbb{U}_{\mathtt{R}}=\frac{1}{2}\begin{pmatrix}0&0&0&0&0&0&0&-2\\0&-1&1&0&0&1&1&0\\0&1&0&-1&1&0&1&0\\0&0&-1&1&1&1&0&0\\0&0&1&1&1&-1&0&0\\0&1&0&1&-1&0&1&0\\0&1&1&0&0&1&-1&0\\-2&0&0&0&0&0&0&0\end{pmatrix}\right]\frac{\varphi^n+1}{\varphi^{n/2}} \quad (8)$$

$$\mathbb{U}^{odd(n)}-\mathbb{U}^{-odd(n)}=\left[\mathtt{u}\mathbb{U}_{\mathtt{L}}=\frac{1}{2}\begin{pmatrix}-2&0&0&0&0&0&0&0\\0&1&1&0&0&1&-1&0\\0&1&0&1&-1&0&1&0\\0&0&1&1&1&-1&0&0\\0&0&-1&1&1&1&0&0\\0&1&0&-1&1&0&1&0\\0&-1&1&0&0&1&1&0\\0&0&0&0&0&0&0&-2\end{pmatrix}\right]\frac{\varphi^n-1}{\varphi^{n/2}} \quad (9)$$

Matrix powers of $\mathtt{u}\mathbb{U}_{L,R}$ generate the rank 8 Identity matrix with determinants of roots of unity. Interestingly, while $\mathtt{u}\mathbb{U}_L^{1/n}$ produces matrices that always have a 1 in upper-left/lower-right corners, $\mathtt{u}\mathbb{U}_R^{1/n}$ does not. Yet both produce the same n'th root of unity determinant. We can redefine $\mathbb{U}=\frac{1}{2}\left(\varphi^{-3/2}\mathtt{u}\mathbb{U}_L+\varphi^{3/2}\mathtt{u}\mathbb{U}_R\right)$.

$$H_{cp}=x^8-4x^6+6x^4-4x^2+1 \quad (10)$$

$$U_{cp}=x^8-2\sqrt{5}x^6+7x^4-2\sqrt{5}x^2+1 \quad (11)$$

Exploring further, if we take seriously the idea of $\mathtt{cm}\mathbb{U}$ as a Cartan matrix, it can be visualized with its positive roots, weights, heights, and Hasse diagrams as shown in Figs. 15-16. After deleting duplicates generated in the SuperLie[8] analysis of $\mathtt{cm}\mathbb{U}$, the cumulative index count up to height 8 is same as that of E_8 being 120. The Coxeter-Dynkin diagram, with Cartan, Schlafli, and Coxeter matrices shown in Fig. 5 shows that rational scaling on the Identity and Involutory matrices can reproduce cm$\mathbb{U}$.

Generating the $\mathtt{cm}\mathbb{U}$-based vertex coordinates and projecting to 3D using the methods of [7] gives somewhat different results than with the folded E_8 of Fig. 8. Instead of finding each of 56 possible subsets of 3 dimensions having the same tally of hull groupings with the same hull geometries, $\mathbb{U}$ groupings rotate into much smaller groups as shown in Fig. 6.

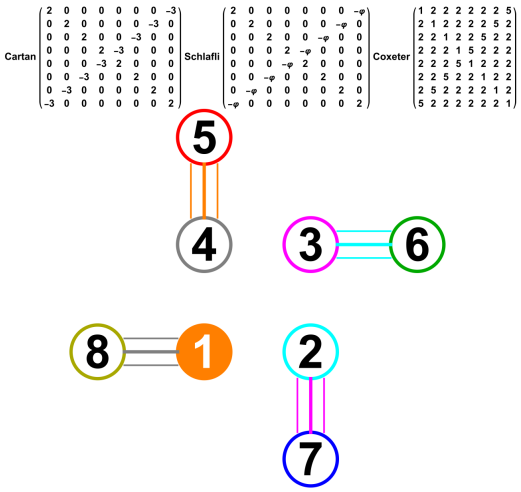

Figure 5: cm$\mathbb{U}$ Coxeter-Dynkin diagram, with Cartan, Schlafli, and Coxeter matrices

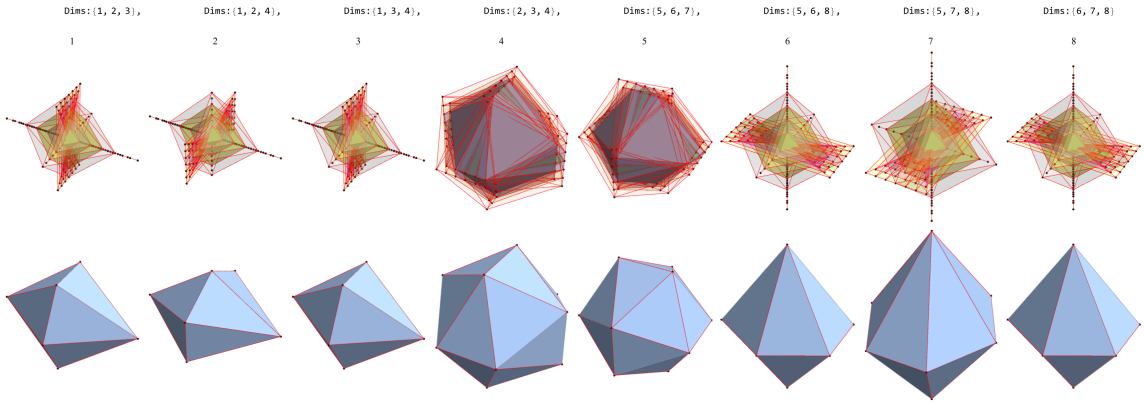

Figure 6: Orthogonal projections to 3D of cm$\mathbb{U}$-based vertices from the ±roots of cm$\mathbb{U}$

4 Discussion

From [3] we know that $\mathbb{U}$ produces the folding of E_8 to H_4 with $\mathbb{U}^{-1}$ involved in the unfolding back to E_8. We also know its palindromic characteristic polynomial coefficients are those shown in (11) with the same form as (10). This gives us a better understanding of why E_8 has an isomorphism to both the Hadamard matrix and H_4. Given that the sum, difference, product, and division of $\mathbb{U}$ and cm$\mathbb{U}$ generate both the left and right matrix identities of rank 8 suggests a possible connection to Bott periodicity.

Since Toffoli and Hadamard matrices and gates are universal for quantum computation[9] [10], this makes the relationship between E_8 and H_4 (by way $\mathbb{U}$ and cm$\mathbb{U}$, u$\mathbb{U}_L$, and u$\mathbb{U}_R$ constructed by them) interesting for QC.

With this new perspective, $u\mathbb{U}$ may be able to be understood as a chiral 8D Real ($\mathbb{R}$) form of what the Complex ($\mathbb{C}$) Pauli (and Dirac) matrices are in 2D (and 4D) as spinors. Further study using hypercomplex forms of $\mathbb{H}$ (and G_2 as the automorphism group of octonions $\mathbb{O}$) for 4D H_4 (and 8D E_8 e.g. using Kirmse closed construction[11]) respectively, is warranted. If a group theoretic E_8 based three generation Standard Model (SM) with particle assignments is shown to be viable[12][13] (e.g. as $\mathbb{R} \otimes \mathbb{C} \otimes \mathbb{H} \otimes \mathbb{O}$ [14][15][16]), this perspective might provide a possible connection between the Fermi-Dirac statistics of fermions (and Bose-Einstein statistics of bosons) originating from the odd (and even) powers of $\mathbb{U}$, as well as provide more detailed implications for QM, Grand Unified Theories (GUTs), such as in CPT symmetry breaking.

5 Conclusion

This paper has presented several notable properties of $\mathbb{U}$ that are shown to be related to the isomorphism between H_4 and E_8. The most significant of these properties is that $\mathbb{U}.\mathbb{U}$ is to rank 8 matrices what the golden ratio is to numbers. This combined with finding the construction of $\mathbb{U}$ from the Pauli and Dirac gamma matrices' relationship to 2-qubit CNOT, SWAP and 3-qubit Toffoli CCNOT and Hadamard matrices informs the understanding of group theoretic quantum mechanics (QM), quantum computing (QC) theory, quantum chemistry, particle physics, and GUTs.

Acknowledgments

I would like to thank my wife for her love and patience and those in academia who have taken the time to review this work.

Funding Statement

Not applicable.

Conflict of Interest

The author declares no conflict of interest.

Institutional Review Board Statement

Not applicable.

Code Availability

A corresponding MTM notebook source code is available on the author's website at: `https://www.TheoryOfEverything.org/TOE/JGM/E8_and_H4_in_QM_and_QC.nb`.

References

[1] Borcherds RE. The Leech lattice and other lattices; 1999.
Available from: `https://arxiv.org/abs/math/9911195`.

[2] Koca M, Al-Ajmi M, Koca NO.
Quaternionic representation of snub 24-cell and its dual polytope derived from E8 root system.
Linear Algebra and its Applications. 2011 feb;434(4):977-89.
Available from: `https://doi.org/10.1016%2Fj.laa.2010.10.005`.

[3] Moxness JG.
The Isomorphism of H_4 and E_8.
ArXiv e-prints mathGR. 2023 Oct.
Available from: `https://arxiv.org/abs/2311.01486`.

[4] Koca M.
E8 Lattice with Octonions and Icosians.
CERN, 1211 Geneva 23, Switzerland. 1989.
Available from: `https://cds.cern.ch/record/197019/files/198906327.pdf`.

[5] Koca M, Koca N.
Quaternionic Roots of E8 Related Coxeter Graphs and Quasicrystals.
Turkish Journal of Physics. 1998 May;22:421-36.
Available from: http://journals.tubitak.gov.tr/physics/issues/fiz-98-22-5/fiz-22-5-8-97022.pdf.

[6] Dechant PP.
The birth of E8 out of the spinors of the icosahedron.
Proceedings of the Royal Society of London Series A. 2016 Jan;472:20150504.
Available from: http://adsabs.harvard.edu/abs/2016RSPSA.47250504D.

[7] Moxness JG.
The Isomorphism of 3-Qubit Hadamards and E_8.
ArXiv e-prints mathGR. 2023 Nov.
Available from: https://arxiv.org/abs/2311.11918.

[8] Grozman P, Leites D.
Lie Superalgebra Structures.
Czechoslovak Journal of Physics. 2004 nov;54(11):1313-9.
Available from: https://doi.org/10.1007%2Fs10582-004-9794-y.

[9] Shi Y. Both Toffoli and Controlled-NOT need little help to do universal quantum computation; 2002.
Available from: https://arxiv.org/abs/quant-ph/0205115.

[10] Aharonov D. A Simple Proof that Toffoli and Hadamard are Quantum Universal; 2003.
Available from: https://arxiv.org/abs/quant-ph/0301040.

[11] Anastasiou A, Hughes MJ. Octonionic D=11 Supergravity and 'Octavian Integers' as Dilaton Vectors; 2015.
Available from: https://arxiv.org/abs/1502.02578.

[12] Wilson RA, Dray T, Manogue CA.
An octonionic construction of E8 and the Lie algebra magic square.
Innovations in Incidence Geometry: Algebraic, Topological and Combinatorial. 2023 sep;20(2-3):611-34.
Available from: https://doi.org/10.2140%2Fiig.2023.20.611.

[13] Wilson RA. On possible embeddings of the standard model of particle physics and gravity in E_8; 2024.
Available from: https://arxiv.org/abs/2404.18938.

[14] Furey N. An Algebraic Roadmap of Particle Theories, Part I: General construction; 2023.
Available from: https://arxiv.org/abs/2312.12377.

[15] Furey N. An Algebraic Roadmap of Particle Theories, Part II: Theoretical checkpoints; 2023.
Available from: https://arxiv.org/abs/2312.12799.

[16] Furey N. An Algebraic Roadmap of Particle Theories, Part III: Intersections; 2023.
Available from: https://arxiv.org/abs/2312.14207.

[17] Fonseca RM.
GroupMath: A Mathematica package for group theory calculations.
Computer Physics Communications. 2021 oct;267:108085.
Available from: https://doi.org/10.1016%2Fj.cpc.2021.108085.

Supplementary Materials

E_8 and H_4 Projections Figs. 7-9

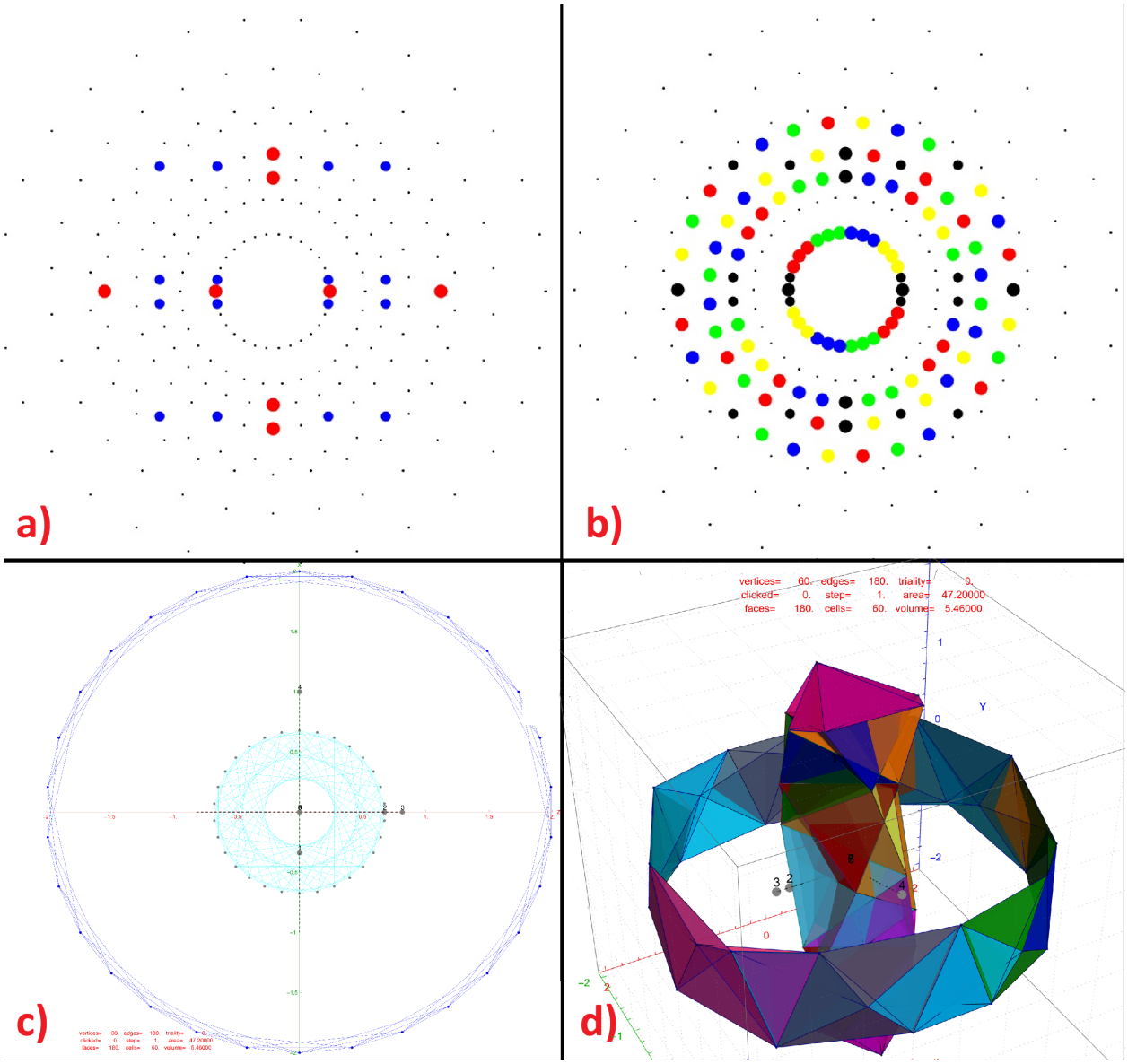

Figure 7: E_8 Petrie projection with H_4 600-cells' substructure in Van Oss projection
a) H_4 24-cell highlighting the 16-cell (red on-axis vertices) and 8-cell (blue off-axis vertices)
b) H_4 Snub 24-cell with four $\pi/5$ rotations of the 24-cell (black) in red, green, blue, yellow
c) φH_4 600-cell 2D projection of 60 vertices and 180 edges in inner/outer rings
d) φH_4 600-cell 3D projection with Boerdijk-Coxeter helices tessellating 3-sphere surfaces

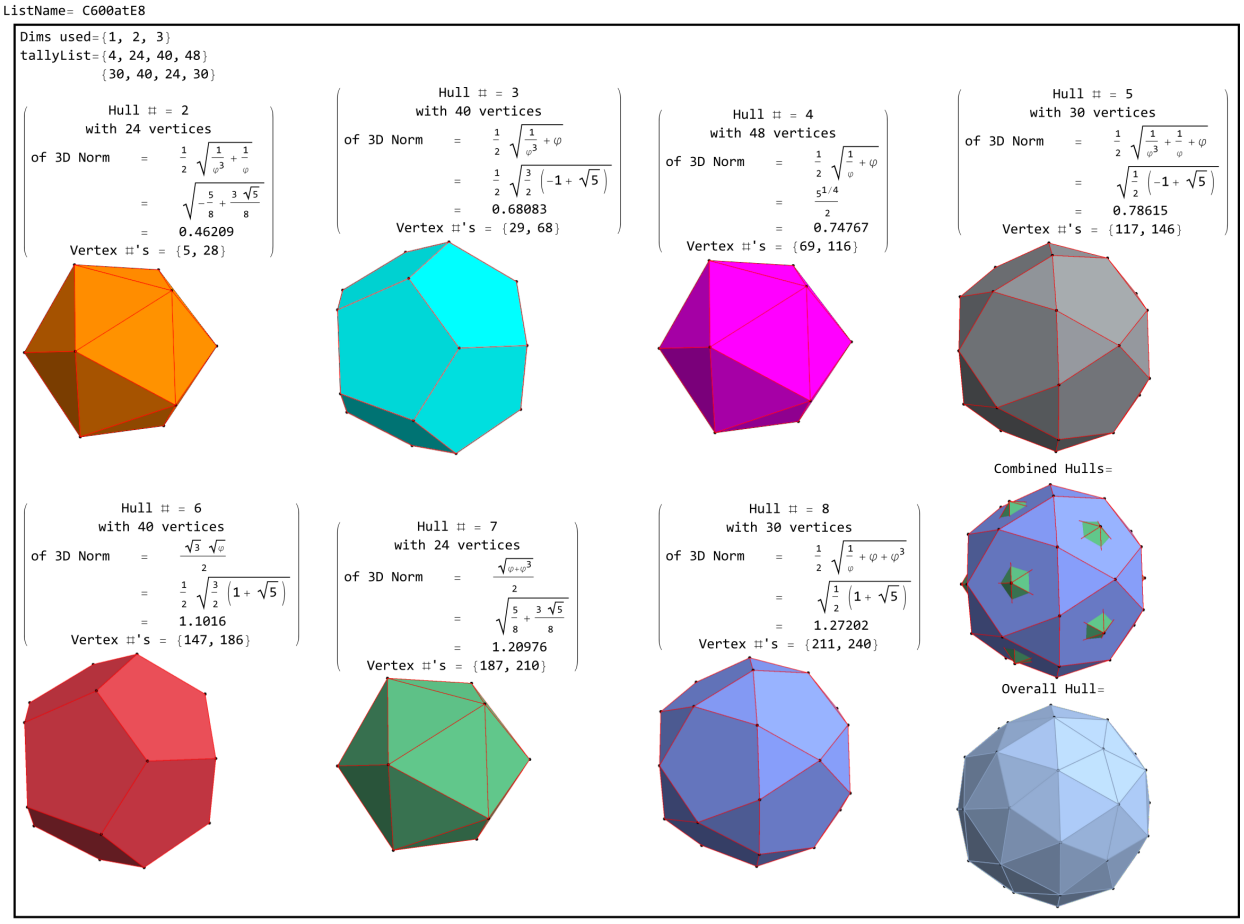

Figure 8: Concentric hulls of 4_{21} in Platonic 3D projection with numeric and symbolic norm distances

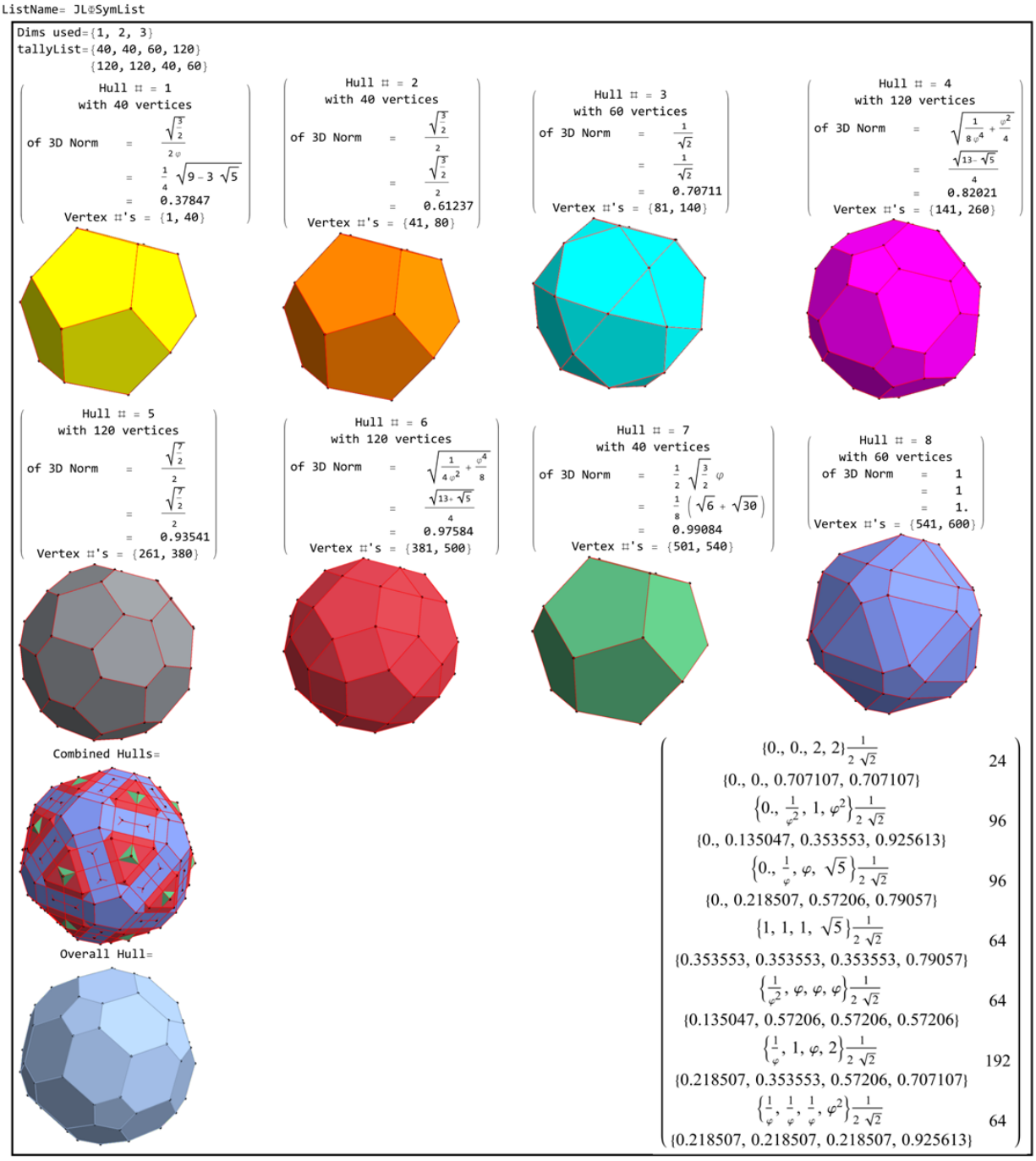

Figure 9: Concentric hulls of J as the tri-rectified H_4 120-cell of order 600 in Platonic 3D projection with numeric and symbolic norm distances. This is generated by $\mathtt{J} = \mathtt{prq}[\mathtt{A}', 1, \mathtt{I}] = \mathtt{prq}[\mathtt{A}', \alpha^{0-4}, \mathtt{T}]$.
Note: The numeric and symbolic tally list of unpermuted vertex values in the lower-right corner

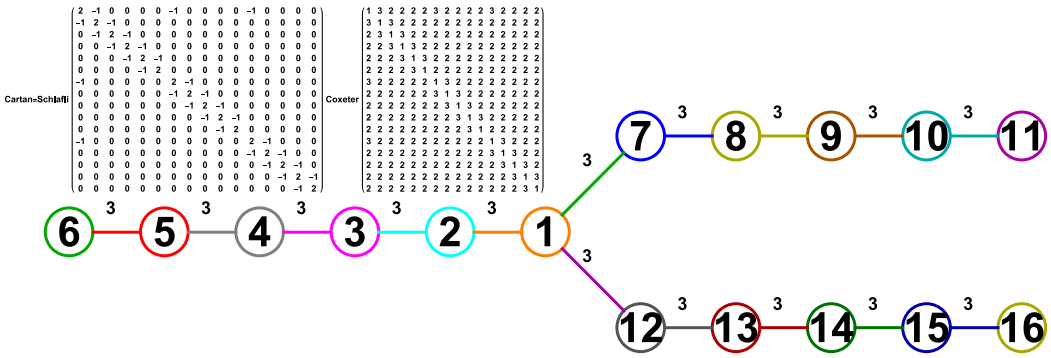

Figure 10: The wreath product of the Monster group with $\mathbb{Z}_2$ ($M \wr \mathbb{Z}_2$) is the BiMonster, a quotient of the Y_{555} Coxeter-Dynkin diagram which contains six $E_8(Y_{124})$ Coxeter-Dynkin diagrams and the 23_{rd} Niemeier lattice E_8^3 root system. This can be reduced to Y_{444} by applying the *spider relation* to E_8^3.

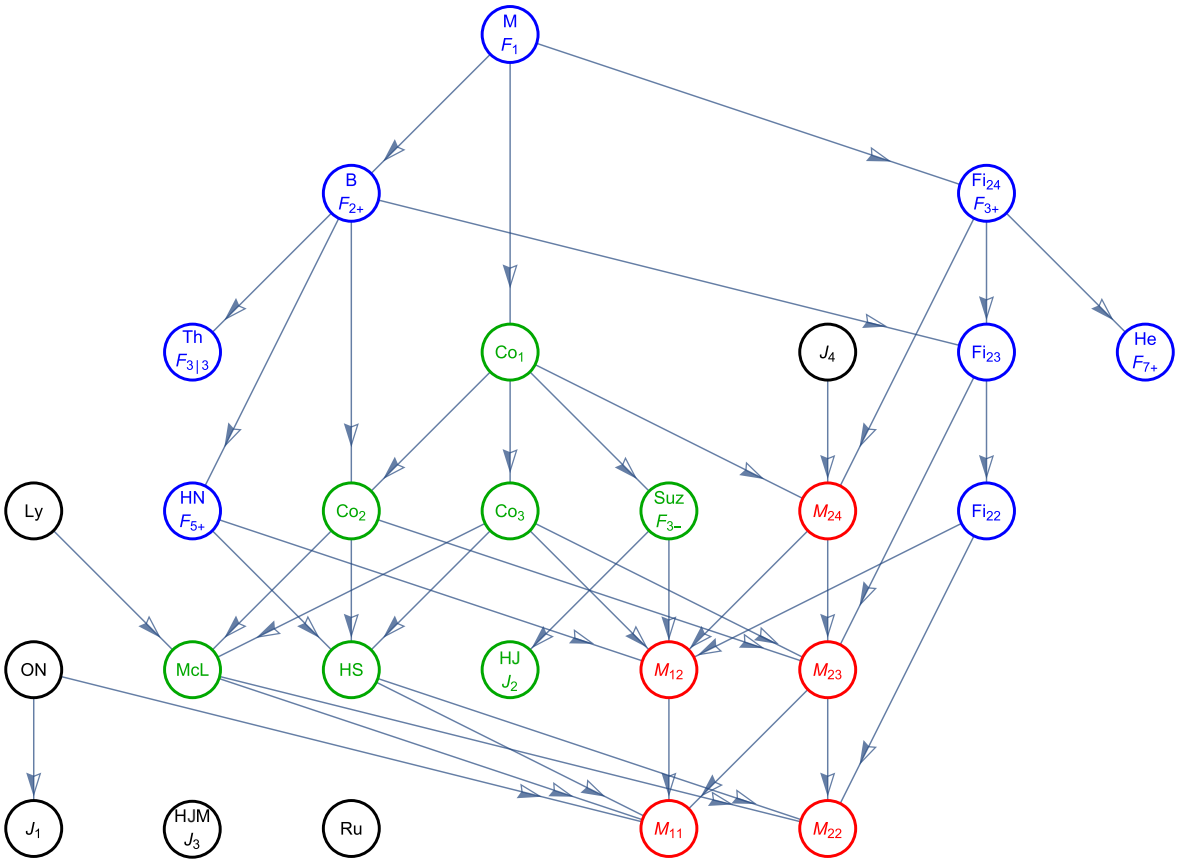

Figure 11: Hasse diagram of sporadic groups in their Monster group sub-quotient relationship. *Happy Family* genarations:
Red=Mathieu groups (1_{st})
Green=Leech lattice groups (2_{nd})
Blue=other Monster sub-quotients (3_{rd})
Black=Pariahs

Row	Lattice root system	Dynkin diagram	Coxeter number	G_0	G_1	G_2	G_∞
1	Leech lattice (no roots)		0	1	$2Co_1$	1	Z^{24}
2	A_1^{24}		2	2^{24}	1	M_{24}	2^{12}
3	A_2^{12}		3	$3!^{12}$	2	M_{12}	3^6
4	A_3^8		4	$4!^8$	2	1344	4^4
5	A_4^6		5	$5!^6$	2	120	5^3
6	$A_5^4D_4$		6	$6!^4(2^34!)$	2	24	72
7	D_4^6		6	$(2^34!)^6$	3	720	4^3
8	A_6^4		7	$7!^4$	2	12	7^2
9	$A_7^2D_5^2$		8	$8!^2(2^45!)^2$	2	4	32
10	A_8^3		9	$9!^3$	2	6	27
11	$A_9^2D_6$		10	$10!^2(2^56!)$	2	2	20
12	D_6^4		10	$(2^56!)^4$	1	24	16
13	E_6^4		12	$(2^73^45)^4$	2	24	9
14	$A_{11}D_7E_6$	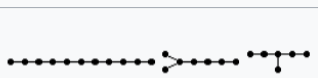	12	$12!(2^67!)$ (2^73^45)	2	1	12
15	A_{12}^2		13	$13!^2$	2	2	13
16	D_8^3		14	$(2^78!)^3$	1	6	8
17	$A_{15}D_9$		16	$16!(2^89!)$	2	1	8
18	$A_{17}E_7$	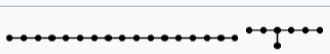	18	$18!(2^{10}3^45.7)$	2	1	6
19	$D_{10}E_7^2$		18	$(2^910!)$ $(2^{10}3^45.7)^2$	1	2	4
20	D_{12}^2		22	$(2^{11}12!)^2$	1	2	4
21	A_{24}		25	$25!$	2	1	5
22	$D_{16}E_8$	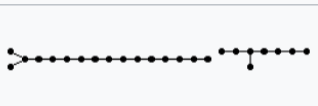	30	$(2^{15}16!)$ $(2^{14}3^55^27)$	1	1	2
23	E_8^3	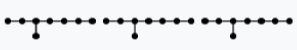	30	$(2^{14}3^55^27)^3$	1	6	1
24	D_{24}		46	$2^{23}24!$	1	1	2

Table 2: Niemeier Lattice Table

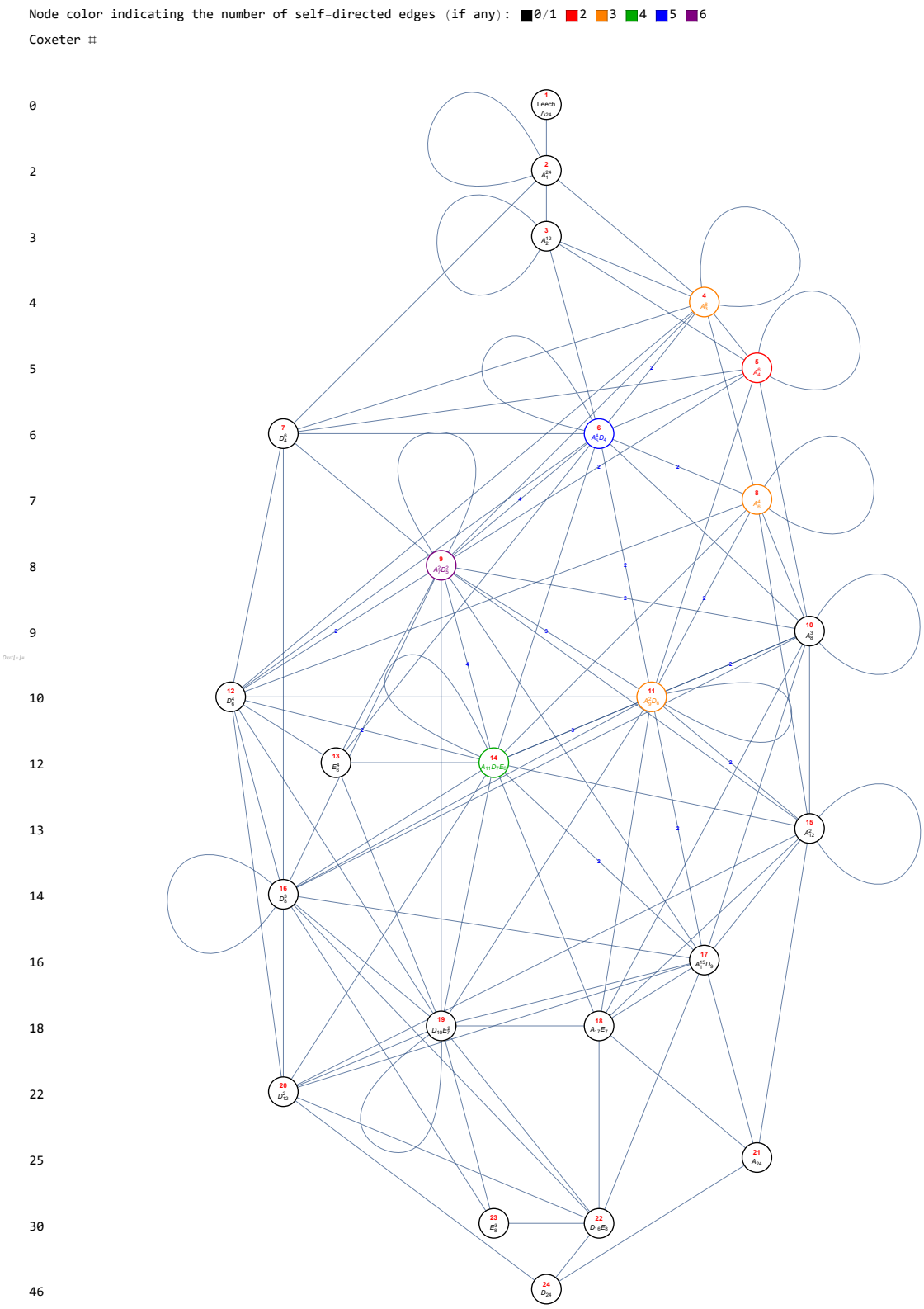

Figure 12: Kneser neighborhood graph of Niemeier lattices
Each color coded node represents one of the 24 Niemeier lattices, and the lines joining them represent the 24-dimensional odd unimodular lattices with no norm 1 vectors.
The Coxeter number of the Niemeier lattice is to the left.
The red node index number indicates the row in Table 2.

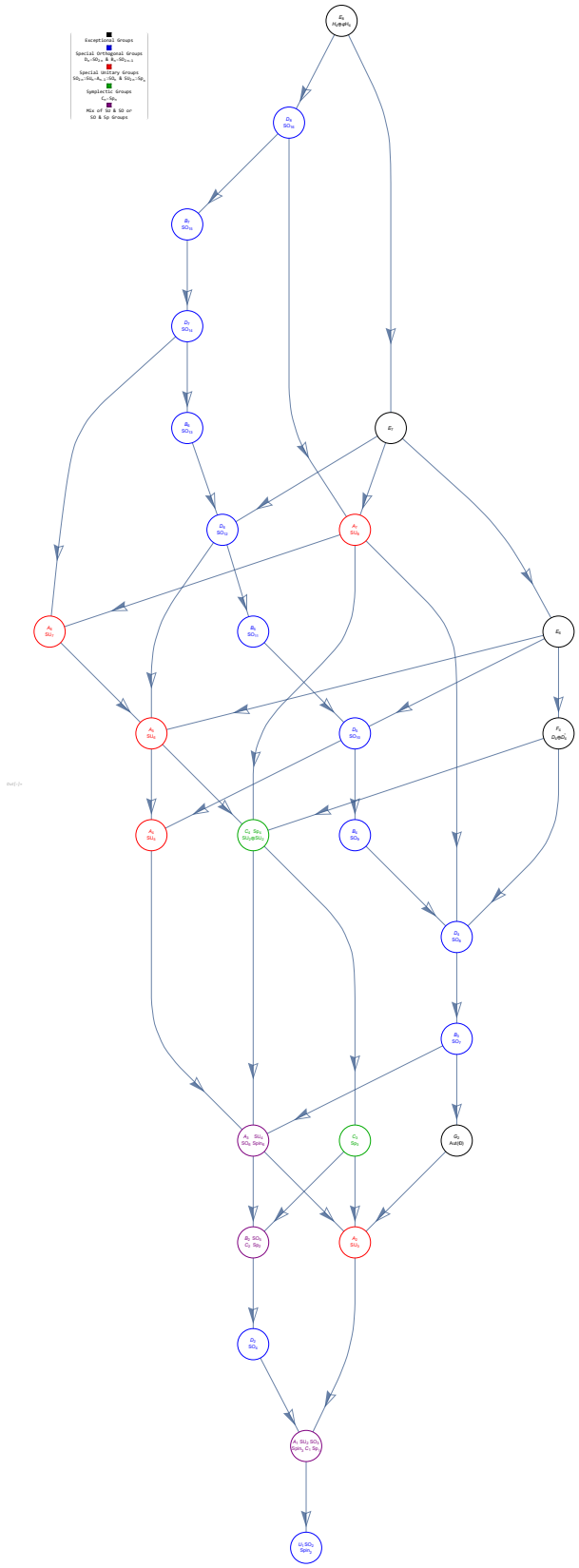

Figure 13: E8 subgroup tree as a directed Hasse diagram
The height of the Lie algebra on the diagram approximately corresponds to the rank of the algebra.
Note: A line from an algebra down to a lower algebra indicates that the lower algebra is a subalgebra of the higher algebra.

Maximal embeddings of E_8 at height 248 Fig. 14

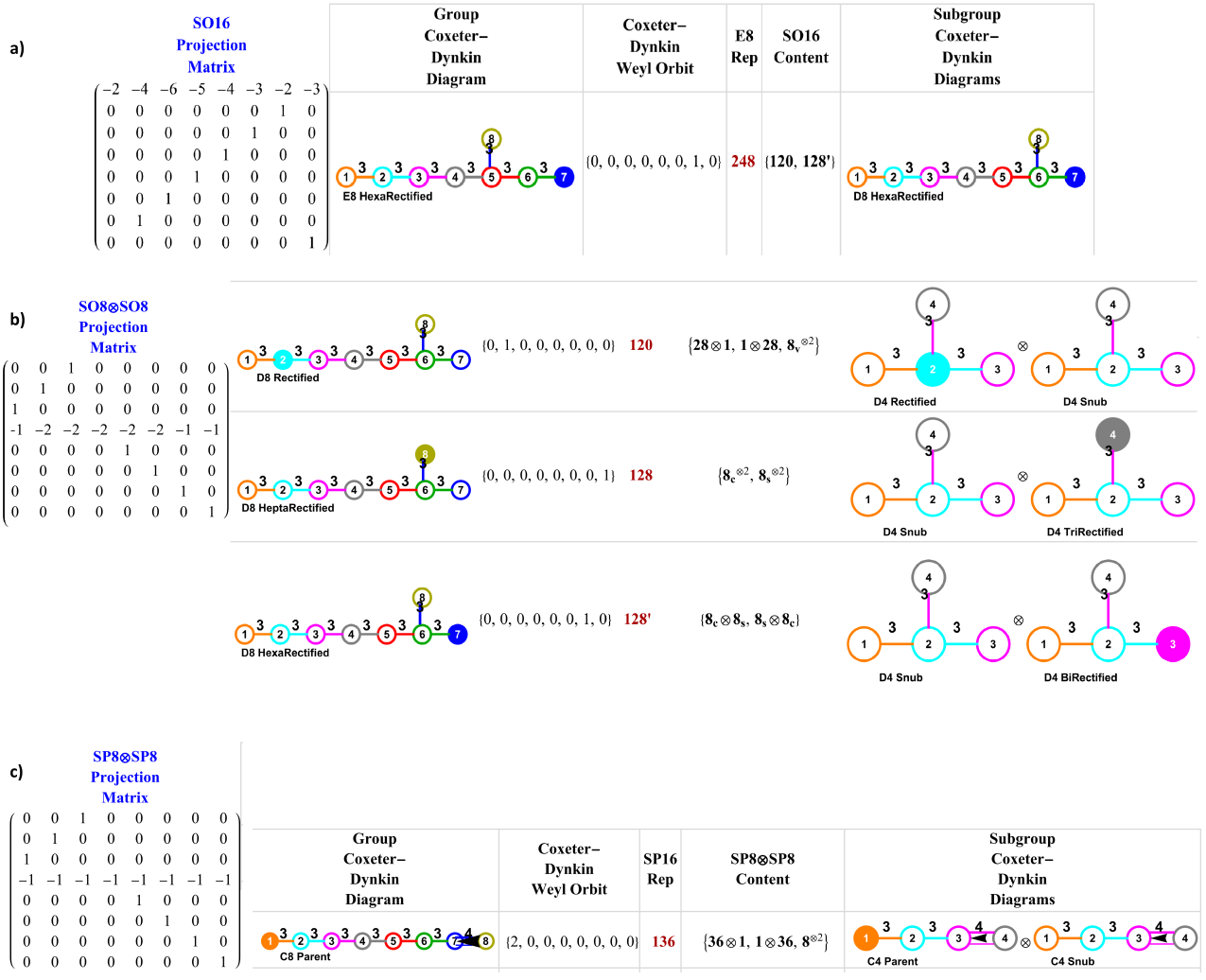

Figure 14: E_8 maximal embeddings at height 248 of content SO(16)≅D_8 (120,128')
a) Height 248 SO(16) content 120=(112+4+4)+128'
b) Height 120 and 128' SO(8)⊗SO(8) content w/$8^{\otimes 2}_{v,c,s}$ triality
c) Height 136 Sp(8)⊗Sp(8) content (32+4)⊗1, 1⊗(32+4), $8^{\otimes 2}$
Note: This output was created in *Mathematica*™ with support from the GroupMath[17] and SuperLie[8] packages.

Analysis of cmU Figs. 15-16

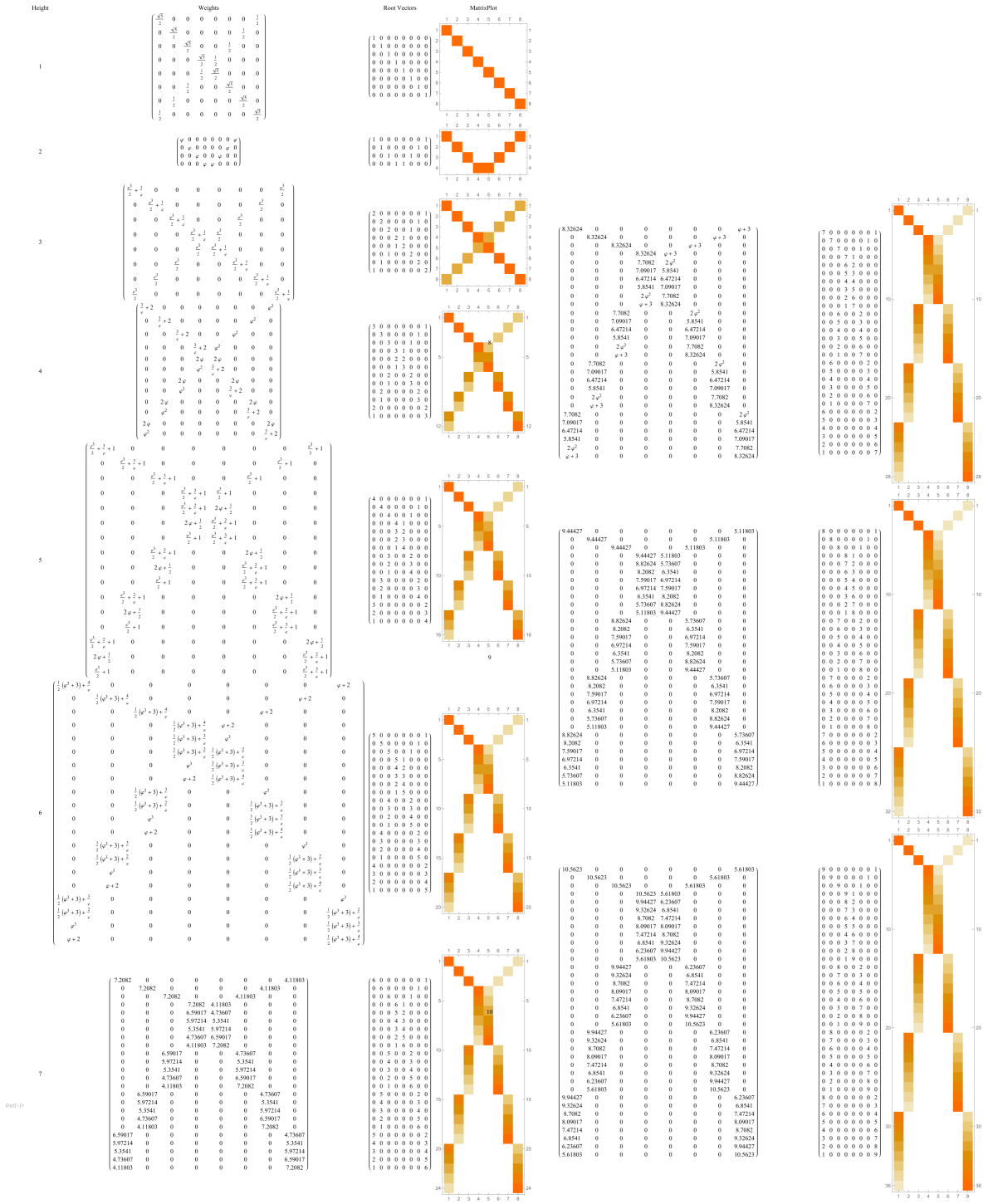

Figure 15: Analysis of cmU showing the cumulative height group indices, positive roots, weights, and heights
Note: At height 8 the cumulative index count is 120, giving 240 positive and negative roots as in E_8

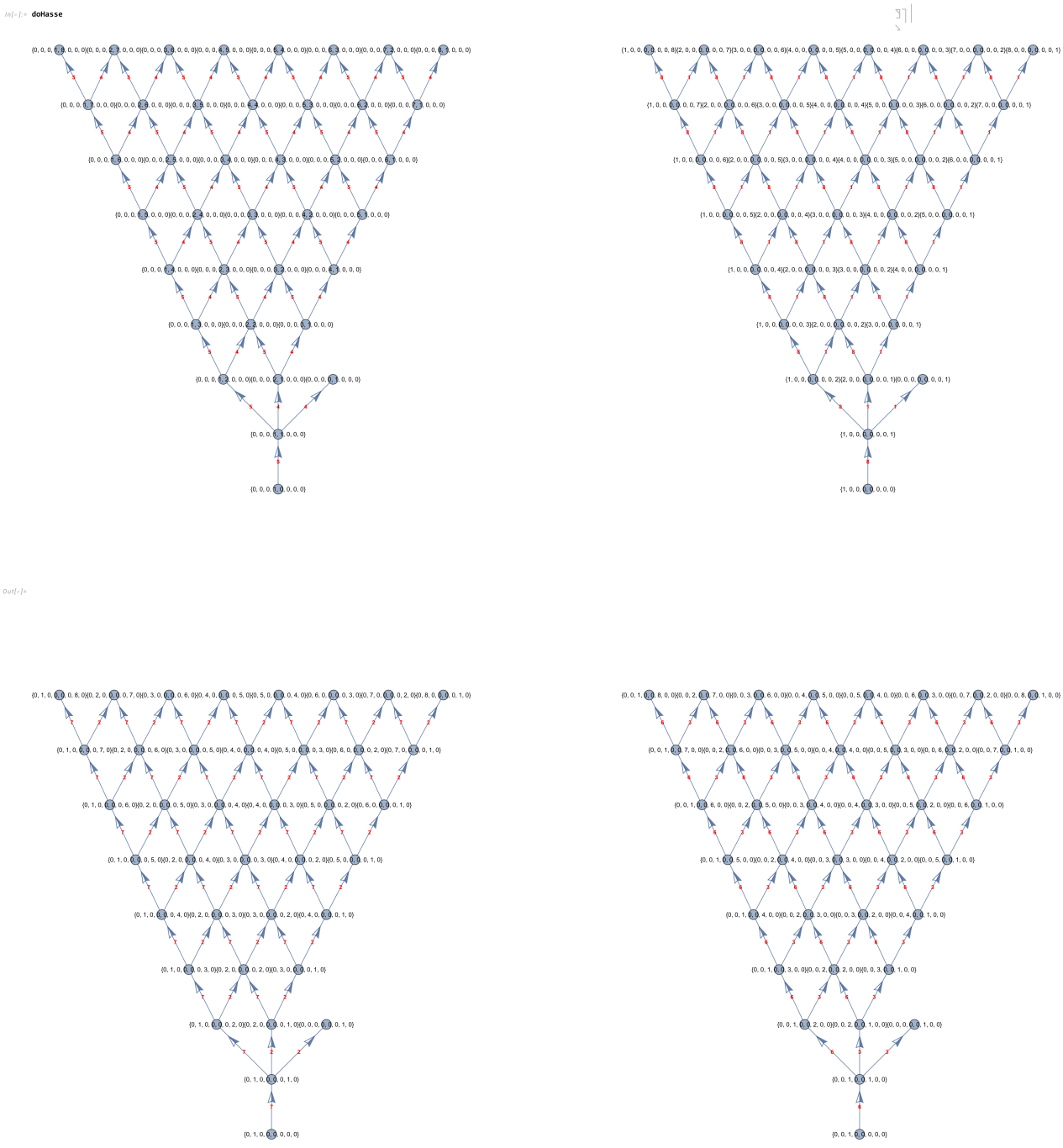

Figure 16: Analysis of $\mathtt{cm}\mathbb{U}$ showing its Hasse visualizations up to height 8
Note: At height 8 the cumulative index count is 120, giving 240 positive and negative roots as in E_8